

Atomic structure of a decagonal Al-Pd-Mn phaseMarek Mihalkovič,¹ Johannes Roth,² and Hans-Rainer Trebin^{2,*}¹*Institute of Physics, Slovak Academy of Sciences, 84511 Bratislava, Slovakia*²*Institut für Theoretische und Angewandte Physik, Universität Stuttgart, 70550 Stuttgart, Germany*

(Received 4 September 2017; published 8 December 2017)

We present a detailed structure solution for the 16-Å decagonal quasicrystal in the Al-Pd-Mn system by means of cluster decoration and *ab initio* energy minimization. It is based on structure models of the ε and other approximant phases. The ε phases can be represented as subsets of a hexagon-boat-star (HBS) tiling. The decagonal phase comprises further HBS tiles. We have constructed several fictitious HBS approximants and optimized their structures individually. All tiles are decorated by two types of atomic clusters: the pseudo-Mackay icosahedron (PMI) and the large bicapped pentagonal prism (LBPP). It turns out that, whereas the PMI clusters can be kept essentially unchanged, the LBPP clusters must be adjusted in occupancy with Al atoms depending on their positions in the various tiles. In this way we obtain cluster decorations for all tiles of the decagonal quasicrystal. The calculations were confirmed by evaluation of an effective tile Hamiltonian.

DOI: [10.1103/PhysRevB.96.214103](https://doi.org/10.1103/PhysRevB.96.214103)**I. INTRODUCTION**

Soon after the discovery of icosahedral quasicrystals by Shechtman *et al.* [1] it was found that quasiperiodicity is not limited to icosahedral phases. Many other alloys were synthesized whose diffraction patterns exhibited an eightfold, tenfold, or 12-fold rotational symmetry. These systems show characteristics of both usual crystals and quasicrystals: They possess quasiperiodic layers that in the perpendicular direction are stacked periodically. This unique feature of two different order principles shows up in anisotropies of transport properties, such as electrical or thermal conductivity or diffusivity.

Of these two-dimensional quasiperiodic phases the decagonal quasicrystals (d-QCs) have been studied the most in the past years, mainly due to the successful growth of large single crystals of high perfection (millimeter size, for example, for d-AlCuCo [2]). Depending on the lattice parameter along the periodic direction, d-QCs are divided into four classes: 4-, 8-, 12-, and 16-Å quasicrystals. A convenient way to describe the structure of these materials is in terms of two-dimensional tilings. The tilings are obtained by projecting centers of characteristic cluster columns along the periodic direction. The diameters of these clusters vary for each d-QC and range between a few Å's up to ≈ 20 Å. Thus, d-QCs are characterized roughly by their structural building units and the assembly thereof. Their detailed atomic structure, however, is still unknown and not yet completely understood, mainly due to their large degree of inherent structural and chemical disorders.

Essentially, there are two different experimental methods to investigate the structures of such highly complex materials: high-resolution transmission electron microscopy (HRTEM) and hyperspace crystallography. Although HRTEM—acting in real space—obtains resolutions up to 0.5 Å and is able to distinguish Pd and Mn, there are uncertainties in resolving aluminum positions of which most d-QCs are composed [3]. Nevertheless, it plays an indispensable role in obtaining the skeleton structures of two-dimensional quasicrystals. In

hyperspace crystallography the quasicrystal is treated as a periodic structure embedded in a higher-dimensional space into which the reciprocal wave vectors of the measured Bragg peaks are lifted [4,5]. Similar to conventional crystallography, the refinement captures only the average structure and does not resolve correlations existing among atoms.

In this paper we present an *ab initio*-based structure solution of the (metastable) 16-Å-periodic decagonal Al-Pd-Mn quasicrystal, described experimentally in Ref. [6]. The phase consists of eight atomic layers stacked with 16-Å periodicity. Alternatively, it can be characterized by columns of icosahedral clusters along the periodic direction whose projections form a so-called hexagon-boat-star (HBS) tiling. Other stable 16-Å-periodic decagonal quasicrystals have been discovered in the systems Al-Ni-Ru [7] and Al-Ir-Os [8].

In a previous work we established a structure model for the ε_6 phase by cluster decoration of hexagon tiles [9]. We found that its structure is best described by two clusters: the pseudo-Mackay icosahedron (PMI) and the large bicapped pentagonal prism (LBPP). The decoration was extended to tiles of the ε_{16} phase. Our objective is to extend it further to general HBS tilings. For that purpose, we construct several fictitious approximants containing such HBS tiles, decorate them with PMI and LBPP clusters, and energy optimize the system by varying the occupancy of the component clusters. In this way we obtain a decoration rule for each cluster depending on its position in the various tiles. Hence, we arrive at a structure model for the decagonal Al-Pd-Mn quasicrystal.

This paper is organized as follows: In Sec. II we briefly review the ε phases and their relationship to the d-QC of Al-Pd-Mn. The binary HBS tiling is described in Sec. III along with the computational methods we employed. The general decoration for the HBS tilings and thus the structure of the d-QC is presented in Sec. IV.

II. ε PHASES OF AL-PD-MN**A. Atomic structure**

The family of orthorhombic ε phases consists of a variety of crystalline structures exhibiting very similar diffraction

*trebin@itap.uni-stuttgart.de

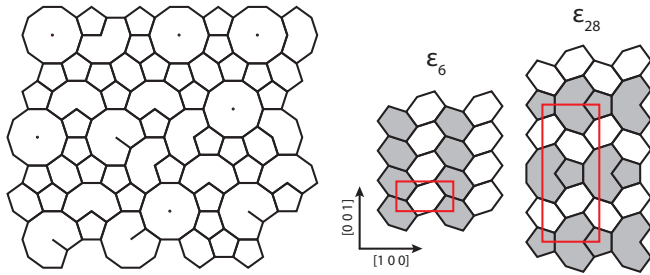


FIG. 1. Idealized tiling representation of the 16-Å d-QC (left panel). The tiling vertices (that we identify with the centers of the columns of PMI clusters) correspond to bright spots in the HRTEM image of the 16-Å d phase [6]. Right panel: Two high-temperature equilibrium tilings observed in the Al-Mn-Pd system [10], ϵ_6/ξ' (pure hexagons) and $\epsilon_{28}/\xi'_2/\Psi$, which is an intergrowth of ϵ_6/ξ' with ϵ_{16}/ξ'_1 . The linkages' length—separation between neighboring PMI columns—is 7.6 Å.

patterns [10]. The phases conveniently are designated ϵ_l where $l = 6, 16, 22, 28, \dots$ refers to the index $(00l)$ of the first strong diffraction spot. All phases feature the same lattice parameters of about 23.5 Å along the [100] direction and 16.5 Å along the [010] direction. The lattice parameter along [001] depends on the particular phase and varies between 12.6 Å for the ϵ_6 phase and about 82 Å for ϵ_{40} .

The structures of the ϵ phases are best described by PMI clusters, stacked on top of each other forming cluster columns along the [010] direction. The projections of these columns along the stacking direction form two-dimensional tilings consisting of hexagons, pentagons, and nonagons. The ϵ_6 phase is the smallest member containing 304 atoms in the unit cell and having a composition of $\text{Al}_{73.7}\text{Pd}_{22.4}\text{Mn}_{3.9}$ [9]. Its tiling is composed of hexagons only (see Fig. 1). The tilings of the higher indexed ϵ_l phases ($l > 6$) also contain nonagon and pentagon tiles. One denotes them ξ'_n , too, where $n - 1$ is the number of hexagon rows in between the nonagon-pentagon rows. ϵ_{28} frequently is called the Ψ phase. The gaps in between the PMI columns are filled in all phases with glue atoms in the form of LBPPs.

The PMI and LBPP clusters are illustrated in Figs. 2 and 3, respectively. The PMI cluster consists of three shells surrounding a central Mn atom. The first shell comprises nine Al atoms forming a tricapped trigonal prism with D_3 symmetry. The outer two shells are composed of 12 Pd atoms

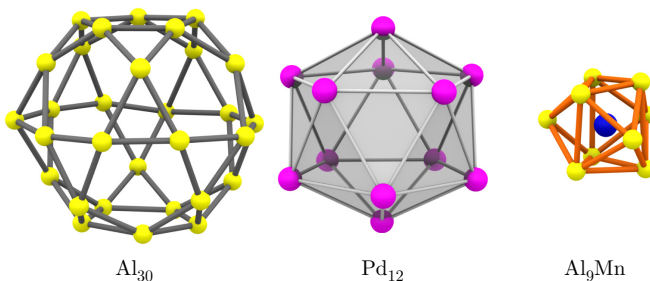


FIG. 2. PMI cluster consisting of three atomic shells: Al_{30} icosidodecahedron, Pd_{12} icosahedron, and an Al_9Mn inner shell.

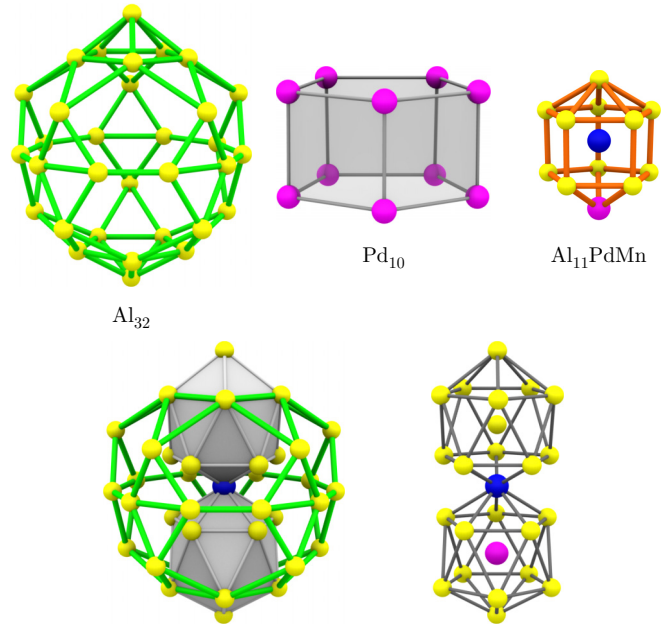


FIG. 3. Top: LBPP cluster consisting of three atomic shells: Al_{32} icosidodecahedron-type shell, Pd_{10} pentagonal prism, and an $\text{Al}_{11}\text{PdMn}$ inner shell. Bottom: Alternative cluster description.

in the form of an icosahedron and 30 Al atoms in the form of an icosidodecahedron.

The LBPP cluster similarly is composed of three shells, including a central Mn atom. The inner shell comprises 11 Al atoms and one Pd atom as illustrated in Fig. 3 (top right). This shell is surrounded by a pentagonal prism of Pd atoms and an icosidodecahedron-type shell composed of 32 Al atoms. Alternatively, the atoms of the inner and outer Al shells can be divided into two small icosahedra, stuck together by the central Mn atom and embedded in an Al_{30} icosahedral-type shell [cf. Fig. 3 (bottom)]. Most atoms of the LBPP clusters are shared with adjacent PMIs. For instance, in the energy optimized structure model of the ϵ_6 phase only eight atoms of each LBPP are independent and cannot be attributed to any PMI [9].

A fully occupied LBPP cluster contains 55 atoms. In Sec. IV we will show that the occupancies of the LBPP clusters depend strongly on their positions in the various tiles.

B. Relation to the decagonal quasicrystal

The ϵ phases share the same cluster columns with the 16-Å d-QC of Al-Pd-Mn and are similar in composition [6]. A projection of the decagonal phase along the columnar axis yields a tiling with equal edge length but with a variety of tiles not present in any ϵ phase. Its tiling is depicted in Fig. 1. The decagonal phase is metastable and is characterized as a defective tiling of a 7.6-Å edge length. Upon annealing it decomposes into the ϵ phases. Therefore, and due to the structural similarities, the ϵ phases have been considered approximants of the decagonal phase. The tile vertices are decorated with PMI clusters, and the space in-between is almost equivalently filled by LBPP clusters, although, with an extended occupation rule, depending on the particular tile

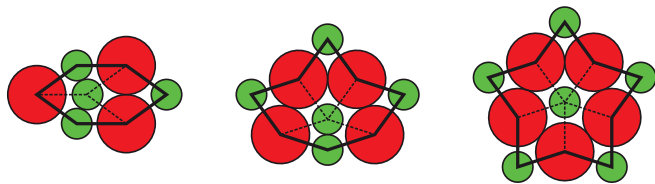


FIG. 4. Hexagon (left), boat (middle), and star (right) tiles with small and large nodes (outlined with green and red circles, respectively).

as will be shown in Sec. IV. Taking into account both types of cluster columns, the decagonal phase can in fact be mapped to a particular tiling featuring two types of vertices: the binary hexagon-boat-star tiling.

III. METHODS

A. Binary HBS tilings

The binary HBS tiling is a special case of the Penrose tiling with reduced matching rules [11, 12]. The Penrose rhombuses are stuck together to form a hexagon, a boat, and a star tile as illustrated in Fig. 4. Two types of vertices are defined: Vertices whose tile angles are an odd multiple of $\pi/5$ are called *large nodes*, and vertices with tile angles that are an even multiple of $\pi/5$ are labeled as *small nodes*. The hexagons, boats, and stars can be assembled only by putting large nodes on large nodes and small nodes on small nodes.

Associating the columns of the PMI clusters with the large nodes and the columns of the LBPP clusters with the small nodes, each ε phase can be mapped to a particular HBS tiling [9]. The tilings of the ε_6 and ε_{16} phases are shown in Figs. 5(a) and 5(b), respectively. The tiling of the ε_6 phase consists of boat tiles only, aligned in staggered orientations [colored white and gray in Fig. 5(a)]. The characteristic tiling of ε_6 formed by hexagons is retrieved by connecting adjacent large nodes in the HBS tiling [superimposed by red lines in Fig. 5(a)]. All other vertices are small nodes and coincide with the positions of the LBPP cluster columns (partially highlighted by green dots). To closely reproduce the experimental lattice parameters of the ε phases along the [001] and [100] directions, we set the edge lengths of the Penrose rhombuses in all HBS tiles to 6.6 Å [9]. In this paper we designate each approximant by the number of hexagon (*H*), boat (*B*), and star (*S*) tiles in its primitive unit cell. Hence, ε_6 will be referred to as B_2 .

The purpose of this paper is to establish a decoration rule applicable to any HBS tiling, thus incorporating all realizable next-neighbor interactions between PMI and LBPP clusters, and yielding the energetically most favorable atomic structure. We constructed several model approximants, each containing distinct cluster interactions, and energy optimized their atomic structures. The approximants studied in this paper are illustrated in Fig. 5. An essential difference between them is the arrangement and length of the chains of the small nodes. Whereas the hexagons of ε_6 contain only two neighboring small nodes, resembling the characteristic alternating stacking of the LBPP clusters, the other tiles, such as the nonagons inside the H_2S tiling of ε_{16} consist of sequences of five small nodes [Fig. 5(b)]. In the atomic structure this results in new

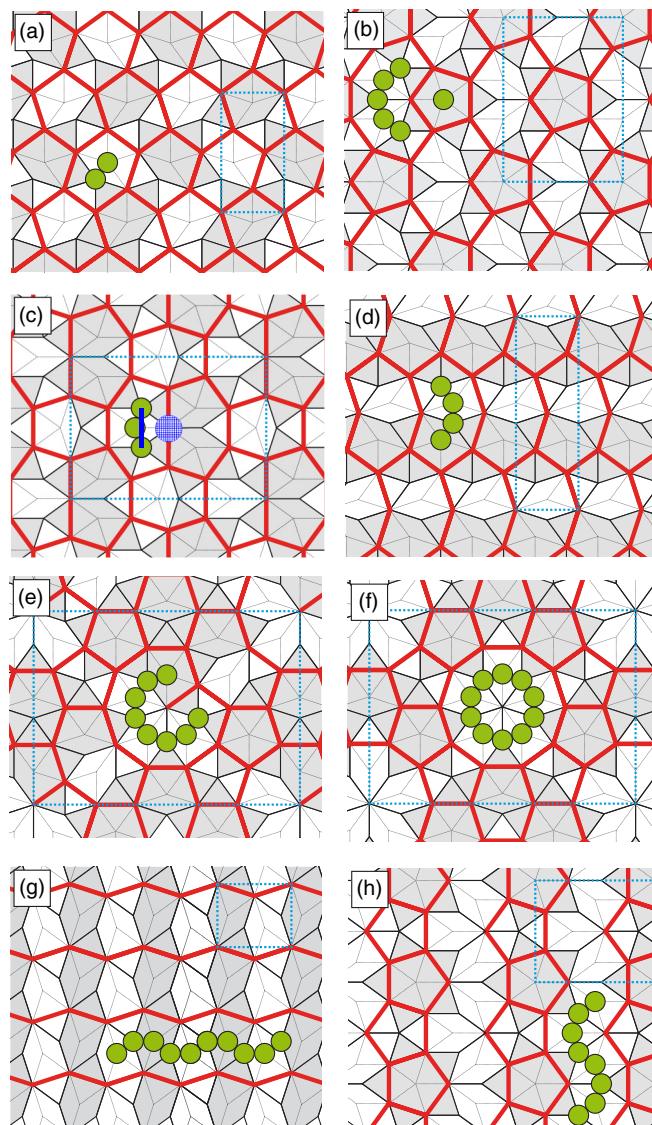


FIG. 5. Binary HBS tilings of the approximants studied in this paper. Vertices of the superimposed red tilings constitute the large nodes of the underlying HBS tilings. They indicate the positions of the PMI columns. All other vertices are small nodes and specify the positions of the LBPP cluster columns of which some are outlined by green circles. The dotted rectangles highlight the unit cells. (a) B_2 , (b) H_2S , (c) HB_3 , (d) HB , (e) H_4B_3S , (f) H_5BS_2 , (g) H_2 , and (h) H_3S . In (c) the blue line segment and the blue-hashed circle characterize tiling objects for an effective tile Hamiltonian as discussed in Sec. IV.

horizontal interactions between the LBPP clusters, leading to a partial cluster interpenetration not present in the ε_6 phase. Figures 5(c)–5(f) show further approximants with other tiles that have been observed in the decagonal phase of Al-Pd-Mn. We also considered tilings containing infinite chains of small nodes across periodic boundaries [Figs. 5(g)–5(h)] that, in the end, once a decoration rule is set up, will let us construct numerous variations of the above-mentioned tiles.

Our decoration rule creates a one-to-one correspondence (up to orientations of inner PMI shells) between abstract tilings and atomic configurations: Indeed, given *any* binary tiling, there will be a unique structure with plausible energy. Thus,

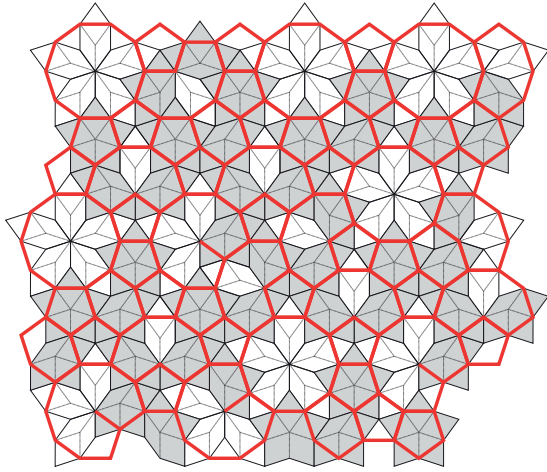


FIG. 6. Binary HBS tiling of the decagonal phase shown in Fig. 1. Vertices of the superimposed red tiling are the large nodes of the underlying HBS tiling; all other vertices are the small nodes. The boat and star tiles of the HBS tiling are shown in gray, and the hexagonal tiles are white.

a quasicrystal with either statistical or perfect decagonal symmetry as in Fig. 6 or periodic tile arrangements representing crystalline ε -type approximants as in Fig. 1 are members of the same decoration-rule family. Favorability of a particular tiling then results from effective *tile interactions*.

B. Energy calculations

The energies of our trial structures are determined in three steps. First, we anneal it with classical molecular dynamics using the embedded atom method (EAM) potentials. The molecular dynamics (MD) simulations are performed with our in-house code IMD [13–15]. Usually we start at about 1000 K (below melting temperature) and slowly cool down to room temperature within 50–100 ps in the NVT ensemble (fixed particle number, volume, and temperature). The EAM potentials we are using have already been developed for our previous study on the ε_6 phase and further improved for this paper. The details of the procedure can be found in Ref. [16]. If necessary, we fix certain atoms during the annealing. We found that in particular Al atoms in the vicinity of the small nodes are quite mobile and start moving between neighboring LBPP clusters which, however, turned out not to be always energetically favored at low temperatures. The annealings are mainly needed in order to relax the Al atoms of the innermost PMI shells as these inner clusters possess certain rotational degrees of freedom [9]. Intercluster interactions have been studied in the literature on simpler systems consisting of inner tetrahedral cages only [17,18]. It was found that the cluster orientations contribute a significant amount to the total energy and depend on the assembly of neighboring clusters. In our case the orientations rely on the formation of the PMI clusters columns and hence vary for each approximant. To circumvent this problem of not knowing *a priori* the optimal orientations, we simply relax each structure into the global energy minimum using the above-described simulated annealing method. Typically, we align randomly the inner shells inside the PMI clusters but always with their threefold

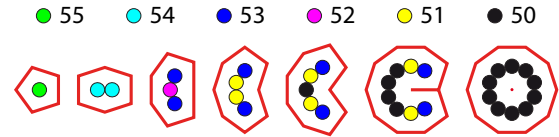


FIG. 7. Tiles with adjusted occupancy of LBPP clusters. The colored circles emphasize the occupancy rules for the LBPP clusters located at the small nodes in the various tiles. A fully occupied LBPP cluster contains 55 atoms.

axis pointing along the [010] direction. Provided that the annealings are started at sufficiently high temperatures and run in sufficiently long times, the atoms move into the lowest-energy state, hence resulting in the optimal orientations of the inner shells [19].

The atoms as well as the volume and the shape of the unit cell afterward are relaxed further using *ab initio* methods. We apply the density functional theory code The Vienna *ab initio* simulation package (VASP) with the projector-augmented-wave method in the Perdew-Wang generalized gradient approximation [20–22]. All calculations are performed until an accuracy of 10^{-3} eV or better is achieved for the total energy. For more details on these calculations we refer to Ref. [9].

The plausibility of a structure is estimated by convex hull calculations. First, we determined the enthalpies of formation of all experimentally known phases of the Al-Pd-Mn phase diagram. The enthalpy of formation is obtained by subtracting the total energies of the pure elemental subsystems from the total energy of a structure. The structures with the lowest enthalpy of formation constitute the vertices of the convex hull in a composition-enthalpy diagram. The enthalpy difference to the convex hull ΔE provides a measure for the stability and hence the quality of the structure. The low-temperature phase diagram for Al-Pd-Mn used in this paper is shown in Fig. 13 of Ref. [9]. The relevant competing phases constituting the convex hull are $\text{Al}_{21}\text{Pd}_8$, Al_3Pd_2 , $T\text{-AlMnPd}$, and the ternary version of the $\text{Al}_{72}\text{Mn}_5\text{Pd}_{18}\text{Si}_5$ phase (recently refined in Refs. [23,24]). Depending on the composition of our trial structures, we calculate the energy differences ΔE relative to the triangle spanned by $\text{Al}_{21}\text{Pd}_8$, Al_3Pd_2 , and $\text{Al}_{72}\text{Mn}_5\text{Pd}_{18}\text{Si}_5$ or Al_3Pd_2 , $T\text{-AlMnPd}$, and $\text{Al}_{72}\text{Mn}_5\text{Pd}_{18}\text{Si}_5$.

IV. RESULTS AND DISCUSSION

Each of our approximants (Fig. 5) was optimized individually using the methods described in Sec. III B. Our starting decoration models were the optimized structures of ε_6 and ε_{16} presented in our previous paper (see Ref. [9]). The PMI clusters (Fig. 2) turn out to be identical. Also the LBPP clusters essentially are unchanged. Within the pentagon they are isolated and contain 55 atoms as in Fig. 3. In the other tiles they form chains. Due to their interaction and their overlaps the number of Al atoms in these neighboring LBPP clusters is changing so that the total number of atoms varies between 50 and 54 as demonstrated in Fig. 7. Figure 8 illustrates the distribution of the LBPP cluster subtypes on the ideal HBS tiles for $d\text{-AlPdMn}$ from Figs. 1 and 6. As discussed later, the key constraint in this step of the optimization comes from the positioning of the Fermi energy E_F near the center of

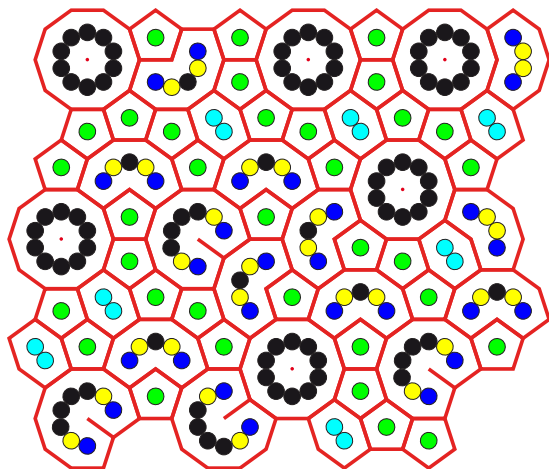


FIG. 8. Tiling of the d-QC with adjusted occupancies of LBPP clusters.

a deep pseudogap in the electronic density of states (DOS). Indeed, the total energy steeply increases for models that either introduce electronic states near E_F or move E_F up or down the pseudogap center.

Table I lists the compositions, formation enthalpies, and deviations from the convex hull of the two $T = 0$ -K stable ternaries, the nearly stable ε_6 (alias ξ') phase, and the hypothetical approximants depicted in Fig. 5, resulting from the final geometry optimization by VASP.

An exemplary final atomic structure is imaged in the left panel of Fig. 9, showing a 6-Å-thick slice through the $H_5B_2S_2$ structure [entry labeled (f) in Table I] with 1048 atoms in the unit cell, viewed parallel to the pseudofivefold direction. The left half of the picture displays the fully optimized structure at $T = 0$ K. Al atoms are depicted in yellow, Pd atoms are depicted in red, and Mn atoms are depicted in blue. The right half shows the spatial occupancies of the same slice from a

TABLE I. *Energetics of approximants of 16-Å-decagonal Al-Pd-Mn.* ΔH 's are *ab initio* formation enthalpies, ΔE energy differences to the convex hull of stable crystalline phases, and ΔE_{fit} are the energy differences fitted by a “tile Hamiltonian” discussed in the text. The last column shows the correspondence of table lines with tilings in Fig. 5. The two $T = 0$ -K stable ternary phases are labeled by their Pearson symbols: *oP156* for T -AlMnPd phase and *oP168* for $Al_{72}Mn_5Pd_{18}Si_5$.

Structure	N_{at}	%		eV/at.			
		Al	Mn	ΔH	ΔE	ΔE_{fit}	
<i>oP168</i>	168	76.2	19.0	-0.4635	Stable		
<i>oP156</i>	156	79.5	5.1	-0.2996	Stable		
B_2/ε_6	304	73.7	3.9	-0.5165	0.3	0.8	(a)
H_2S/ε_{16}	399	73.9	4.0	-0.5089	2.7	4.3	(b)
HB	246	74.0	4.0	-0.5060	4.2	4.6	(d)
HB_3	550	73.8	4.0	-0.5071	6.7	6.6	(c)
H_3S	494	74.1	4.0	-0.5010	7.3	6.4	(h)
H_4B_3S	1044	73.95	4.02	-0.5027	8.5	5.2	(e)
H_5BS_2	1048	74.04	4.01	-0.5010	8.6	8.8	(f)
H_2	188	74.5	4.2	-0.4902	9.6	10.8	(g)

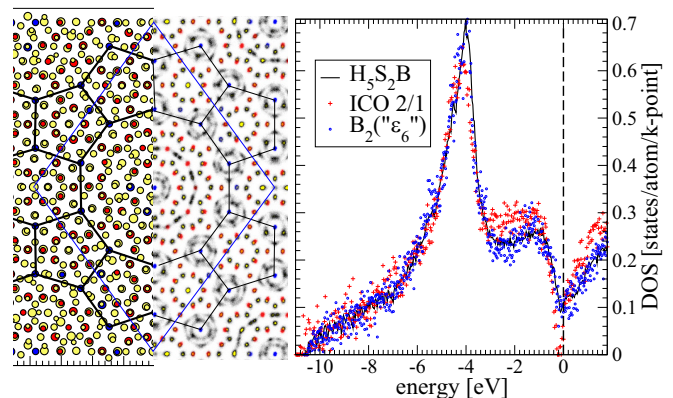


FIG. 9. *Left panel:* A slice parallel to the pseudofivefold axis through the H_5S_2B approximant structure. The left part of the image shows the relaxed static structure. Al atoms are depicted in yellow, Pd atoms are depicted in red, and Mn atoms are depicted in blue. The black lines connect PMI cluster centers (7.6-Å linkages), and the blue lines outline the primitive cell. The right side shows the occupancy probability gathered over ~ 4 -ns MD simulation time at 1200 K. Up to 0.4 occupancy probability, Al atoms are shown as gray-level white to black, above this value they are shown as yellow. The red points indicate the positions of the Pd atoms, and the blue points indicate the positions of the Mn atoms, both above 0.5 occupancy. *Right panel.* (*e*-DOS) comparing the approximants B_2 and H_5BS_2 with a 128-atom cubic approximant of an icosahedral phase [28].

4.3-ns time-averaged MD annealing simulation at 1200 K. Up to 0.4 occupancy probability, the Al atoms are shown as gray-level white to black, above this value they are shown as yellow. The red points indicate the positions of the Pd atoms, and the blue points indicate the positions of the Mn atoms, both above 0.5 occupancy.

Features striking the eye are dark smeared areas within the inner shells of the PMI clusters, centered by Mn atoms (vertices of the pentagonal tiling in the figure). The inner PMI shells are Al_9Mn “nine clusters” in the form of tricapped trigonal prisms, caged by the outer $Al_{30}Pd_{12}$ PMI shell with approximate icosahedral symmetry (see Fig. 2). The threefold axis of the prisms points either along fivefold or twofold icosahedral directions and causes symmetry breaking, providing extra configurational degrees of freedom. In Ref. [25] the complex, quasi-crystal-related $Al_{11}Ir_4$ compound was analyzed whose cubic lattice was decorated with PMI clusters. For their entirely analogic configurational degrees of freedom an entropy of $k_B \ln 9$ per PMI cluster was found. We expect that around 1000 K this entropy decreases the free energy of PMI-based compounds by ~ 6 meV/atom. In light of 2–10 meV/atom instability of our hypothetical approximants vs stable non-PMI crystalline competitors, the PMI entropic configurational entropy should stabilize a wide range of PMI compounds (and we still neglect related vibrational entropy, harmonic and anharmonic).

So far we discussed the relative stability of the decagonal quasicrystal approximant family against competing crystalline phases. Under the assumption of the full integrity of the tiles up to high temperatures (a sufficient energy gap existing between tiling and nontiling configurations), we fit the approximant energies by an effective *tile Hamiltonian* [26] in the spirit of

Ref. [27]. Our calculated approximant energies ΔE_{fit} relative to the convex hull (column 7 of Table I) are a sum of selected tiling objects discussed below: $\Delta E_{\alpha} = \sum_i c_i n_{i\alpha}$ where the index α runs over the approximants (rows of Table I) and c_i , respectively, are energy coefficients associated with the tiling object labeled i . This way, we can effectively express the energy of *any* tiling in terms of local tiling objects.

After trying several possibilities, we find that the optimal effective Hamiltonian is expressed best in terms of four tiling objects: ($i = 1$) small binary Penrose tiling vertices hosting LBPP columns. These are shown as green circles in Figs. 5(a)–5(h); ($i = 2$) *second*-neighbor linkages in the chains of the LBPP columns. One such linkage is shown as a blue line segment in Fig. 5(c); an ($i = 3$) triplet of PMI clusters forming a straight line. The central PMI in such a configuration is marked by the blue-hashed circle in Fig. 5(c); an ($i = 4$) decagon supertile as in the center of Fig. 5(f). The Hamiltonian does not explicitly include columns of PMI clusters, their count is fixed by the tiling, and their energy can be thought of as zero reference. The fitted coefficients were as follows: $c_1 = 0.06$, $c_2 = 0.45$, $c_3 = 2.3$, and $c_4 = 4.4$ eV with a rms deviation of 1.4 meV/atom over the set of structures in the database. The single outlier is the energy of the H_4B_3S tiling [case (e)], which is predicted lower by more than 3 meV/atom.

The robust fit parameters are c_1 and c_2 , related to the number density (c_1) and connectivity (c_2) of the LBPP clusters, and they are both positive. They just reconfirm the apparent observation that longer chains of LBPP columns are disfavored in 16-Å d -AlMnPd—and this is the immediate reason why neither random nor ideal 16-Å decagonal ordering is stable. The other two coefficients adapt the Hamiltonian to special cluster column arrangements: Straight-line linkage between pairs of PMI clusters (HB_3 tiling) correct energies of H_4B_3S or of the special high-symmetry PMI cluster column at the center of the decagon supertile. A small or even negative coefficient c_4 should be indicative of the system with a stable and well-ordered decagonal phase.

We conclude that our modeling captures the observed stability trends: It confirms metastability of the 16-Å d phase; selects the B_2 tiling as the most favorable and nearly stable at $T = 0$ K; and it selects the ε_{16} H_2S structure as the second best. Indeed the experimentally observed ε_{28} phase from the rightmost panel of Fig. 1 is an intergrowth of ε_6 and ε_{16} .

The electronic density of states (e -DOS) of the 16-Å decagonal approximant models exhibits a deep depression near the Fermi energy E_F , indicating the prominent role of the optimal electron-per-atom ratio $e/at.$ in the stabilization of PMI alloys. The structural architecture provides two adjustment controls for shifting E_F : One of them is the number

of Al atoms in the innermost PMI shells: The structure is mechanically stable for a broad range of 8–11 atoms per cluster. Another option is a similar atom-vacancy competition in the chains of the LBPP clusters' columns. We find that the energy is minimized for exactly nine-atom PMI shells and the LBPP cluster occupancy rules expressed in Fig. 7. The e -DOS of the lowest-energy ε_6/ξ' structure, along with the large $H_5B_3S_2$ model shown in the right panel of Fig. 9, share a similar deep e -DOS depression, except the former has more structure. For comparison, we also plotted the e -DOS of a model of a cubic 128-atom approximant of an icosahedral quasicrystal [28]. In this case the pseudogap is even deeper and extends down to practically zero e -DOS.

V. SUMMARY

In a previous article [9] we had proposed a structure model for the ε_6 - and ε_{16} -approximant phases of the 16-Å decagonal quasicrystal in the Al-Pd-Mn system. It was based on a decoration of a planar periodic tiling consisting of staggered hexagons for ε_6 and of pentagons and nonagons for ε_{16} with columns of PMI and LBPPs. These tiles can also be represented as combinations of HBS tiles. They contain large nodes, occupied by the PMI, and small nodes, occupied by the LBPP clusters. Here we have established eight periodic structures containing these tiles, decorated them with the cluster columns, and energy optimized them with molecular dynamics and *ab initio* relaxation methods. The deviations of the energies from the convex hull of stable compounds in the vicinity of the phase diagram are in the meV/at. range and indicate stability. The values were confirmed by evaluation of an effective tile Hamiltonian. It turned out that the decoration of the large nodes with PMI columns remained unchanged whereas in the columns above the small nodes the number of Al atoms in the LBPP clusters had to vary depending on the tile. Applying these decorations to a basic random HBS tiling we arrived at a detailed atomistic structure model for the decagonal Al-Pd-Mn quasicrystal.

ACKNOWLEDGMENTS

This work has been supported by Deutsche Forschungsgemeinschaft, Paketantrag “Physical Properties of Complex Metallic Alloys” (PAK 36). M.M. acknowledges support from the Slovak grant agency under Contracts No. APVV-15-0621 and VEGA No. 2/0082/17. Part of the *ab initio* calculation (high-precision calculation of the electronic DOS of the 1048-atom structure) was performed on supercomputer CC-SAS Bratislava, acquired in Projects No. ITMS 26230120002 and No. 26210120002 and funded by ERDF. We thank B. Frigan for strong support of the calculations.

[1] D. Shechtman, I. Blech, D. Gratias, and J. W. Cahn, *Phys. Rev. Lett.* **53**, 1951 (1984).
 [2] S. Taniguchi and E. Abe, *Philos. Mag.* **88**, 1949 (2008).
 [3] A. Yasuhara and K. Hiraga, *Philos. Mag.* **95**, 1511 (2015).
 [4] T. Janssen, *Acta Crystallogr., Sect. A: Found. Crystallogr.* **42**, 261 (1986).

[5] A. Yamamoto, *Acta Crystallogr., Sect. A: Found. Crystallogr.* **52**, 509 (1996).
 [6] W. Sun and K. Hiraga, *Philos. Mag. A* **73**, 951 (1996).
 [7] W. Sun and K. Hiraga, *Philos. Mag. Lett.* **80**, 157 (2000).
 [8] S. Katrych, T. Weber, M. Kobas, L. Massüger, L. Palatinus, G. Chapuis, and W. Steurer, *J. Alloys Compd.* **428**, 164 (2007).

- [9] B. Frigan, A. Santana, M. Engel, D. Schopf, H.-R. Trebin, and M. Mihalkovič, *Phys. Rev. B* **84**, 184203 (2011).
- [10] M. Heggen, M. Engel, S. Balanetsky, H.-R. Trebin, and M. Feuerbacher, *Philos. Mag.* **88**, 507 (2008).
- [11] F. Lançon and L. Billard, *J. Phys.* **49**, 249 (1988).
- [12] M. Widom, K. J. Strandburg, and R. H. Swendsen, *Phys. Rev. Lett.* **58**, 706 (1987).
- [13] For more information on IMD see also <https://github.com/itapmd/imd> and <http://imd-doc.sourceforge.net/wiki/doku.php>
- [14] J. Stadler, R. Mikulla, and H.-R. Trebin, *Int. J. Mod. Phys. C* **8**, 1131 (1997).
- [15] J. Roth, F. Gähler, and H.-R. Trebin, *Int. J. Mod. Phys. C* **11**, 317 (2000).
- [16] D. Schopf, P. Brommer, B. Frigan, and H.-R. Trebin, *Phys. Rev. B* **85**, 054201 (2012).
- [17] P. Brommer, F. Gähler, and M. Mihalkovič, *Philos. Mag.* **87**, 2671 (2007).
- [18] W. Choi, C. L. Henley, and M. Mihalkovič, [arXiv:1212.5583](https://arxiv.org/abs/1212.5583).
- [19] Local relaxation methods, such as conjugate gradients, usually fail because of the energy barriers existing between different intracluster orientations.
- [20] G. Kresse and J. Hafner, *Phys. Rev. B* **47**, 558 (1993); G. Kresse and J. Furthmüller, *ibid.* **54**, 11169 (1996).
- [21] G. Kresse and D. Joubert, *Phys. Rev. B* **59**, 1758 (1999).
- [22] J. P. Perdew and Y. Wang, *Phys. Rev. B* **45**, 13244 (1992).
- [23] R. Simura, N. Kaji, K. Sugiyama, and K. Hiraga, *Philos. Mag.* **91**, 2603 (2011).
- [24] S. Balanetsky, G. Meisterernst, M. Heggen, and M. Feuerbacher, *Intermetallics* **16**, 71 (2008).
- [25] M. Mihalkovič and C. L. Henley, *Phys. Rev. B* **88**, 064201 (2013).
- [26] M. Mihalkovič, W. J. Zhu, C. L. Henley, and M. Oxborrow, *Phys. Rev. B* **53**, 9002 (1996).
- [27] M. Mihalkovič, J. Richmond-Decker, C. L. Henley, and M. Oxborrow, *Philos. Mag.* **94**, 1529 (2014).
- [28] M. Mihalkovič (unpublished).